Proceedings of the ASME 2019
Internal Combustion Engine Division Fall Technical Conference
ICEF2019
October 20-23, 2019, Chicago, IL, USA

ICEF2019-7241

THERMOCHEMICAL AND SENSIBLE ENERGY RECUPERATION USING THERMALLY-INTEGRATED REACTOR AND DIESEL-AMMONIA DUAL FUELING STRATEGY

Seamus P. Kane, Darrick Zarling, William F. Northrop*
University of Minnesota
Department of Mechanical Engineering
Minneapolis, MN 55455

ABSTRACT

Anhydrous ammonia produced using wind power on farms can be a renewable alternative to conventional fertilizers and to fossil fuels used in engine-powered equipment. Although it has been shown that ammonia can be used in dual fuel modes in diesel engines, its inherently low flame speed results in poor combustion efficiency and thus reduces allowable diesel fuel replacement ratios. In this work, a novel method using a thermochemical recuperation (TCR) reactor system to partially decompose ammonia into hydrogen and nitrogen over a catalyst was demonstrated in diesel engine powered tractor. In the experiments, a John Deere 6400 agricultural tractor powered by a non-EPA tier-certified 4045TL diesel engine was operated in dual-fuel mode using anhydrous ammonia as the secondary fuel. Liquid ammonia from a tank was vaporized and heated using a series of heat exchangers and partially decomposed to hydrogen gas before being fumigated into the intake manifold. The catalytic TCR reactor utilized both exhaust waste heat and unburned hydrocarbon heating value to drive the ammonia decomposition process. Engine emissions and performance data were collected across a standard 8-mode test. The engine was operated using diesel only and in dual fuel mode with up to 42% replacement of diesel with ammonia on a lower heating value basis. Engine loading was accomplished using a power takeoff (PTO) dynamometer. Measured brake thermal efficiency was improved by up to 5.0% using thermochemical recuperation, and brake specific CO_2 emissions were reduced by up to 44% over diesel-only rates.

Keywords: Ammonia, Dual-Fuel, Thermochemical Recuperation

NOMENCLATURE

AFR	Air-Fuel Ratio
BTE	Brake Thermal Efficiency
CDC	Conventional Diesel Combustion
CE	Combustion Efficiency
CPSI	Cells Per Square Inch
FEF	Fumigant Energy Fraction
FTIR	Fourier Transform Infrared Spectrometer
IMEP	Indicated Mean Effective Pressure
LGA	Laser Gas Analyzer
PTO	Power Take-off
NO_x	Oxides of Nitrogen
SCR	Selective Catalytic Reduction
TCR	Thermochemical Recuperation

1. INTRODUCTION

Anhydrous ammonia is produced industrially for use as agricultural fertilizer and as a chemical synthesis feedstock. Consisting of hydrogen and nitrogen, ammonia is produced using the Haber-Bosch reaction (Eq. 1) at temperatures of 400 °C and pressures of 200 bar.

$$3\,H_2 + N_2 \leftrightarrow 2\,NH_3 \quad \left(-45.8\,\frac{kj}{mol}\right) \qquad \text{(Eq. 1)}$$

Hydrogen for the process is commonly provided by steam reforming natural gas which emits carbon dioxide as a byproduct. Alternatively, hydrogen can be produced renewably using water electrolysis and electric power from solar or wind sources. Small pilot-scale operations have demonstrated the feasibility of renewable ammonia production in this manner [1]. In addition to providing a useful fertilizer from wind power, small pilot plants offer an alternative use for excess electrical power by storing it chemically in the ammonia produced. Excess ammonia production could be reused for its energy content later, by either converting back to hydrogen for fuel cell use, or through direct combustion in vehicles and electric generators.

As a fuel, ammonia is energy dense and flammable, but exhibits poor flame speed and is highly resistant to ignition due to high molecular stability. Its adiabatic flame temperature is 1800 °C, [2] which is lower than most common fuels and retards flame propagation during combustion. Despite this, ammonia has still been previously investigated as a fuel due to its mature

industrial production network and the lack of carbon emissions when burned.

Spark-ignition strategies for ammonia combustion in engines have been extensively studied. For example, some previous work has shown success with ammonia-hydrogen combustion where hydrogen is used to enhance the ammonia flame propagation [3–6]. While the studied engines did not produce noticeable ammonia emissions, oxides of nitrogen (NO_x) production was increased when using the ammonia fuel. Grannell et al. showed that for spark ignition engines, up to 70% of gasoline could be replaced with ammonia if the engine load was kept high [7]. Combustion was found to be unstable with any ammonia fueling at indicated mean effective pressures (IMEP) below 4 bar and at replacement rates beyond 70% for higher IMEP. Haputhanthri studied the capacity for gasoline and alcohol fuels as ammonia emulsions [8]. Dual-fuel combustion was achieved at replacement rates of 61.8 grams of ammonia dissolved within one liter of gasoline or ethanol, solving the issue of carrying separate ammonia fuel. Most similar to the work done here is the work presented by Reiter and Kong [9,10]. An off-highway diesel engine was fumigated with anhydrous ammonia achieving diesel replacement rates over 80 percent. However, exhaust ammonia emissions were greater than 1000 ppm even at low replacement rates, which was due to ammonia's poor flame speed and low reactivity.

One alternative to direct ammonia combustion is to dissociate the fuel into hydrogen and nitrogen catalytically using the reverse Haber-Bosch reaction (Eq. 1). Hydrogen has inherently high adiabatic flame temperature, two orders of magnitude higher than that of ammonia. When burned together with ammonia, hydrogen increases laminar flame speed by a factor of 10 at as low as 30% hydrogen fuel fraction. [11,12] Previous studies [3,13–19] have shown that with the use of a proper catalyst, ammonia can be easily cracked to hydrogen and nitrogen using exhaust-relevant temperatures of 300-600 °C. If exhaust waste heat is used to feed dissociation, it follows that partial conversion of ammonia to hydrogen before combustion will improve both engine thermal and combustion efficiency. To perform this conversion onboard an engine, a compact ammonia reformer is needed.

Compact reforming for engines has been studied and experimentally demonstrated by several groups [20–26]. One challenge for practical implementation of compact reforming systems is effectively integrating heat and energy streams to yield improvements in overall system thermal efficiency. Ammonia requires significantly lower activation temperatures relative to hydrocarbon reforming. Due to this, engine waste heat can be used to produce hydrogen from ammonia and increase ammonia combustion efficiency. Diesel engine brake thermal efficiency is generally between 30 to 40% [27], meaning 60 to 70% of fuel energy is wasted through exhaust and heat transfer processes. More common waste energy recovery systems include turbocharging and thermoelectric generators [28], though the latter suffers from poor thermal efficiency. Using exhaust energy to increase the chemical energy of the fuel is a process known as thermochemical recuperation (TCR). TCR for engines generally involves an endothermic fuel reformation process such as steam reforming or decomposition. The reformed fuel contains greater heating value than the original and can deliver this captured energy back into the thermodynamic cycle. This both lowers rejected heat and net input fuel energy, raising overall thermal efficiency.

The objective of this study was to examine the sensible and chemical energy recovery of a diesel engine equipped to run dual-fuel using anhydrous ammonia in a practical engine system on a vehicle. Ammonia fumigant was partially dissociated catalytically using reclaimed engine waste heat to produce hydrogen. This work examines the energy flows through the system and demonstrates the feasibility of such systems for practical implementation in off-highway diesel-powered equipment.

2. EXPERIMENTAL METHODS

A catalytic reactor was designed to partially dissociate fumigated ammonia into hydrogen as depicted in Figure 1. A schematic of the overall system is given in Figure 2. The reactor was installed in place of the stock exhaust muffler directly downstream from the turbocharger as shown in the system installation photo in Figure 2. Sensible heat from the exhaust as well as chemical energy from unburned fuel in the exhaust provided energy at temperatures appropriate for converting ammonia into hydrogen and nitrogen according to Eq. 1. Additional sensible energy was provided to the ammonia fumigant from engine waste heat streams using a liquid ammonia evaporator and an ammonia-exhaust heat exchanger. The heat exchangers were used to vaporize liquid ammonia and preheat it to exhaust temperatures before introduction to the reactor.

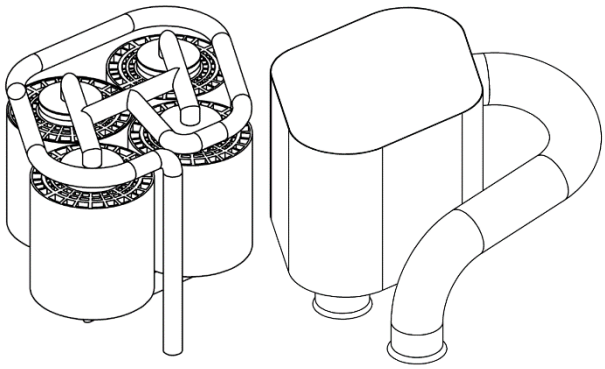

FIGURE 1: INTERIOR ARRANGEMENT OF FOUR CYLINDRICAL CATALYST SECTIONS IN THE TCR REACTOR. EXHAUST ENTERS THROUGH THE FACE FLANGE AND EXITS THROUGH THE CURVED PIPE ON THE RIGHT.

The reactor used in this study consisted of four catalytic assemblies containing an outer oxidation catalyst bound to an inner ammonia decomposition catalyst and separated by a common wall. The monoliths were constructed from FeCrAl metal foil with 300 cells per square inch (CPSI) for oxidation and 600 CPSI for decomposition. The monoliths were wash-coated

with an ammonia decomposition catalyst 4.72% Ru/Al_2O_3 while the outer monoliths were wash-coated with a proprietary rhodium-containing catalyst R44. Both wash-coated catalysts were provided by Johnson Matthey. The sections were welded together such that both exhaust and ammonia flow through parallel sections and in counter-flow to each other to achieve higher rates of heat exchange. A small loop of tubing for ammonia was installed within the exit flow of the exhaust stream to promote further pre-heating before entering the decomposition catalysts. The assembly was insulated externally using rock-wool batts to retain heat and prevent damage to the tractor or engine.

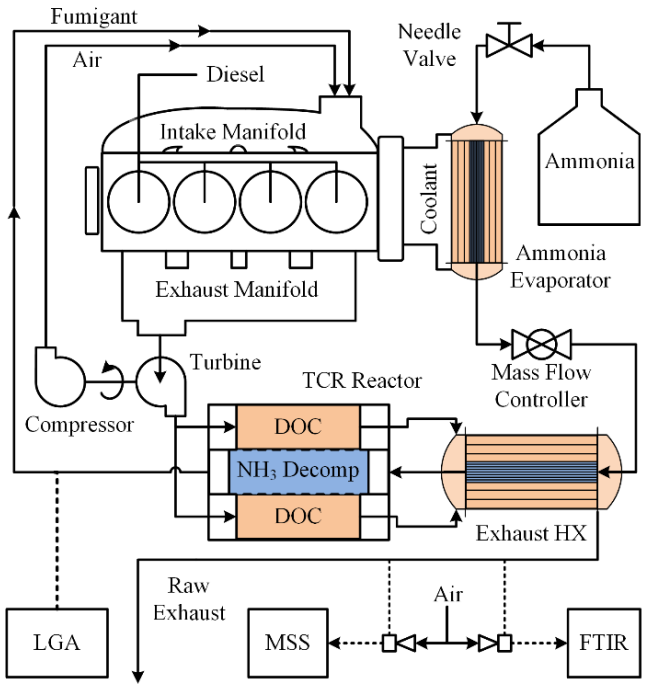

FIGURE 2: SCHEMATIC FOR THE AMMONIA TCR SYSTEM USED IN THIS STUDY. HEAT RECOVERY DEVICES SHOWN IN SEQUENTIAL THERMAL RECOVERY PATH FOR AMMONIA FUEL. DASHED LINES DEPICT SAMPLE PATHS FOR GAS AND PARTICULATE ANALYSIS.

A second custom exhaust heat exchanger assembly was inserted downstream from the reactor to preheat the ammonia as seen in the photo in figure 3. The assembly consisted of two shell and flat-tube EGR coolers assembled in parallel with exhaust in the tubes and ammonia in the shell. The heat exchanger was constructed entirely of 304 stainless steel and is shown in detail in figure 4. The parallel arrangement and open area of the tubes results in negligible flow restriction on the exhaust stream. Exhaust gases again flow in counter-flow to maximize ammonia outlet temperature and thermal recovery.

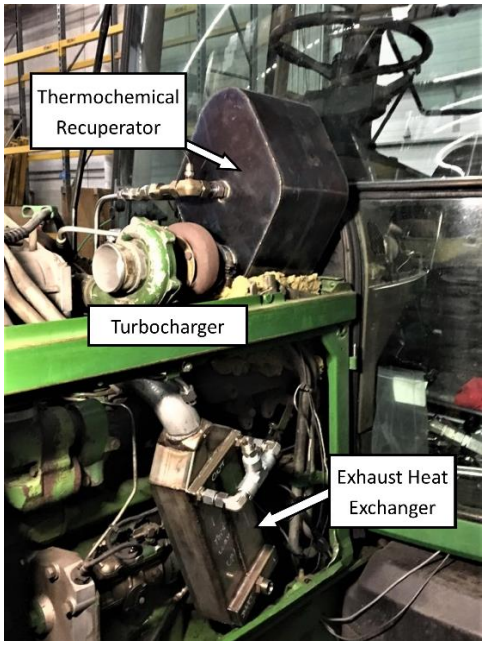

FIGURE 3: TCR REACTOR AND EXHAUST HEAT EXCHANGER SHOWN INSTALLED ON JOHN DEERE 6400 TRACTOR. TURBOCHARGER, REACTOR AND EXHAUST HEAT EXCHANGER ARE LABELED.

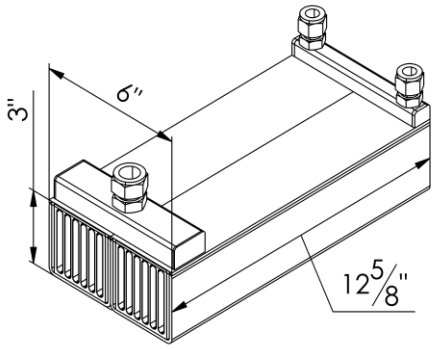

FIGURE 4: DIMENSIONED DRAWING OF THE SECONDARY HEAT EXCHANGE ASSEMBLY. INTERNAL SHELL BAFFLES PREVENT AMMONIA FROM SHORT-CIRCUIT FLOW AND IMPROVE HEAT TRANSFER.

To produce the ammonia vapor needed for this study, liquid withdrawal was necessary. In earlier work, high gas withdrawal rates caused rapid cooling of laboratory cylinders due to ammonia's latent heat of vaporization. This decreased cylinder vapor pressure below that needed for high volume withdrawal. A custom ammonia evaporator was designed such that ammonia's latent heat could be derived from engine coolant. A needle valve was used to throttle the ammonia into the heat exchanger. The resulting drop in pressure caused the ammonia to rapidly cool on the heated fins, producing warmed vapor from engine waste heat. Vapor pressure within the cylinder continues to push ammonia into the system until equalized with the evaporator pressure, or the cylinder is emptied. Coolant flows in a co-flow arrangement with ammonia and is pulled from the engine oil cooler outlet to provide increased temperatures over the engine water jacket.

A 1994 model year John Deere 6400 tractor with JD4045TL engine was used for this study. Engine specifications are listed in Table 1. No emissions aftertreatment was implemented in the tractor's stock configuration. To load the engine, a dynamometer was attached to the tractor's power take-off (PTO) shaft. The PTO shaft rotates in a direct ratio of 1:2.15 with the engine and load torque is controlled at the dynamometer. The PTO dynamometer is a model NEB-600 friction brake device manufactured by AW dynamometers. Engine speed was manually controlled by cab operator using a locking engine throttle hand lever. Load was controlled by hydraulic resistance at the dynamometer and set manually by a separate operator.

Table 1: Engine Specifications

Manufacturer/Model	John Deere 4045TL
Engine Type	4-Stroke DI Diesel
Cylinders	4, in-line
Displacement (L)	4.5
Bore x Stroke (mm)	106 x 127
Compression Ratio	17.0:1
Maximum Power (kW at RPM)	75 at 2200
Aspiration	Turbocharged
Injection System	Inline Distributed Governor
Emissions Certification	Not Certified

The ISO 8178 C1 off-road 8-mode test was used to examine the energy recovery and TCR reactor across all operating conditions. For this engine, the modes and their corresponding loads and speeds are reported in Table 2. Due to low exhaust temperature, mode 8 was not tested using fumigation. This standard provides a weighting factor to assess general emissions from an off-road vehicle, and by extension will provide insight into benefits provided by the dual-fuel strategy and thermal recovery. In addition to the eight modes, each mode was tested with four fumigation rates. The rates of fumigation were decided on a diesel-replacement basis. The fraction of chemical energy provided to the engine when evaluated on a lower heating value basis is known as the fumigant energy fraction (FEF). The values of FEF targeted in this study were 10%, 20%, 30%, and conventional diesel combustion with no fumigation as a baseline (i.e.; 0% FEF). Ammonia fueling was controlled using a Sierra Instruments C100M mass flow controller. Ammonia FEF targets were determined by percentage of conventional diesel fuel consumption, and measured FEF minimally varied from targeted values. Diesel fuel consumption was measured using two Brooks Instruments Oval gear meters attached to the inlet and return from the fuel pump. The net consumption was found by the difference of the two meters over time. The engine controlled fueling using a mechanical governor which maintains constant engine speed for a given throttle position. The governor automatically decreased diesel fueling after introducing fumigant into the intake stream.

Table 2: 8-Mode Test Parameters

Mode	Speed [RPM]	Load [N-m]
1	2200	275
2		210
3		140
4		65
5	1500	310
6		230
7		155
8	1000	0

Temperature was measured using type-K thermocouples installed only at the outlet of each recovery device. Energy recovery rates were calculated using CoolProp, [29] an open-source thermodynamic properties software. Thermochemical recovery was calculated using gas species concentrations measured directly from the thermochemical reactor outlet. Heat exchanger efficiencies were calculated using the ratio of realized heat exchanged over the maximum possible heat exchanged. A Raman-laser gas analyzer by Air Recovery, Inc was used to directly measure the hydrogen and nitrogen components of the fumigant. The remaining fraction was assumed to be ammonia, as no other stable species may be produced from the pure ammonia reactant. Reactor conversion efficiency and reforming efficiency are given in equations 2 and 3, respectively and broadly describe the thermochemical recovery process. Conversion efficiency is the ratio of reacted ammonia to the maximum possible reacted amount. Reforming efficiency describes the ratio of lower heating values of the all fuels in the outlet stream over the fuels in the inlet stream. For ammonia, when the outlet stream is completely converted to hydrogen and nitrogen, the maximum theoretical reforming efficiency is 114.5%. Chemical energy recovery is calculated using the product of reforming efficiency, ammonia mass flow, and lower heating value.

$$\eta_c = \frac{\dot{m}_{NH_3,in} - \dot{m}_{NH_3,out}}{\dot{m}_{NH_3,in}} \quad \text{(Eq. 2)}$$

$$\eta_r = \frac{\sum(\dot{m}_{out} * LHV_{out})}{\sum(\dot{m}_{in} * LHV_{in})} \quad \text{(Eq. 3)}$$

Gaseous and particulate emissions were measured using an AVL Fourier Transform Infrared Spectrometer (FTIR) and AVL MicroSoot sensor, respectively. Both devices sampled from exhaust downstream from all attached recovery devices. Gaseous emissions are thus reported after residence on the oxidation catalyst. Gaseous emissions were diluted 20:1 to prevent over-ranging of ammonia in the FTIR. Soot emissions samples were diluted 5:1 using the dilution system supplied with the MSS instrument. Engine intake air mass flow and total exhaust mass flow rates were calculated using exhaust O_2 concentrations and fuel flow measurements.

3. RESULTS AND DISCUSSION

3.1 Sensible and Latent Heat Recovery

Heat was recovered using the three separate heat exchange devices employed in this system as depicted in figure 2. Of the three, the ammonia vaporizer showed the greatest rates of recovery across all ammonia flows. Figure 5 shows the total sensible and latent recovery by the evaporator versus ammonia flow, and the corresponding heat exchange efficiency. Ammonia vaporization required significant energy over the flow range due to its latent heat. Vaporization took place at the temperature of the liquid tank or lower, due to the downstream pressure in the evaporator being at or below the tank vapor pressure. This generated a consistent temperature differential which enhanced heat transfer rates inside the evaporator. For this reason and due to high boiling heat exchange coefficients, the heat exchange efficiency was consistently above 97% for all tested modes, and ammonia outlet temperatures within 10 °C of the coolant outlet temperatures.

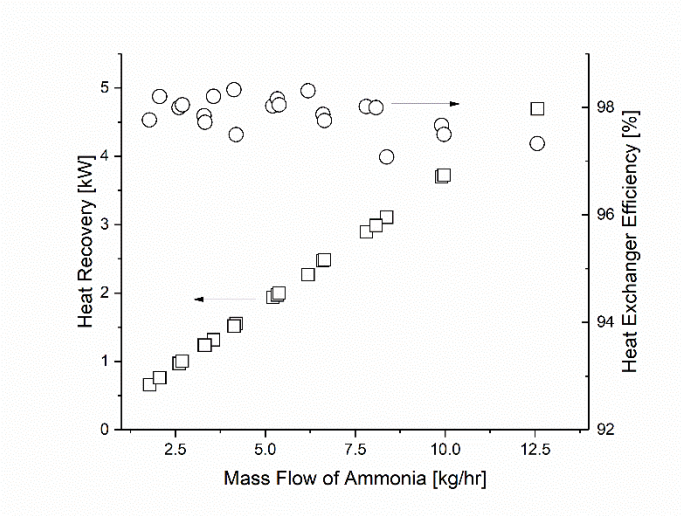

FIGURE 5: HEAT RECOVERY RATE AND HEAT EXCHANGER EFFICIENCY FOR THE AMMONIA VAPORIZER.

The ammonia-exhaust heat exchanger had heat transfer rates and efficiencies that were lower than the evaporator. Recovered energy increased with increasing ammonia flow, as internal convection coefficients of the ammonia increased. Heat exchanger efficiency decreased with increased flow, causing outlet ammonia temperatures to decrease. Figure 6 shows the recovery rate and efficiency of the ammonia-exhaust heat exchanger. The purpose of the device was not to create maximum heat recovery, but to serve as a secondary ammonia pre-heating system to assist catalytic decomposition over the catalyst. The achieved heat exchange efficiencies of 40-60% were acceptable for this reason, as any heat recovered in the device was not needed from within the TCR reactor.

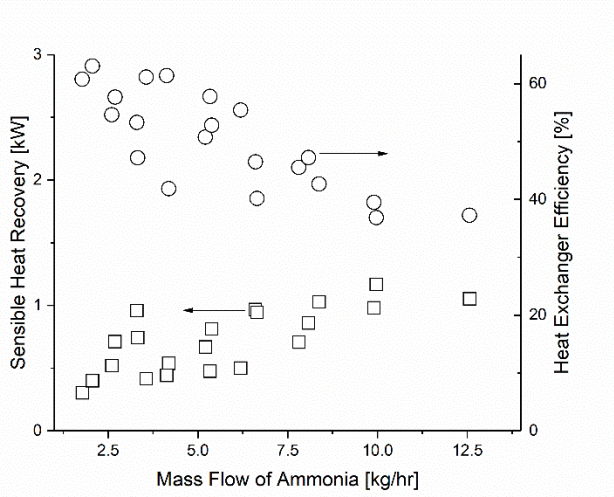

FIGURE 6: HEAT RECOVERY RATE AND HEAT EXCHANGER EFFICIENCY FOR THE AMMONIA-EXHAUST HEAT EXCHANGER

The sensible recovery within the TCR reactor is plotted in figure 7 along with heat exchange efficiency. The heat exchange efficiency appears to plateau near 60% efficiency with increasing ammonia flow. Increased ammonia flow is accompanied by increased engine fueling rates, power output, and exhaust temperatures. Increasing ammonia and exhaust flow enhanced convective heat transfer, but the short residence time at high flows counteracted this. The data indicate that for this reactor, decreased residence time may overwhelm higher heat transfer rate at ammonia flows greater than 12.5 kilograms per hour. Heat recovery trends non-linearly upward, as heat transfer rates are enhanced by the increased temperature difference at higher fueling rates.

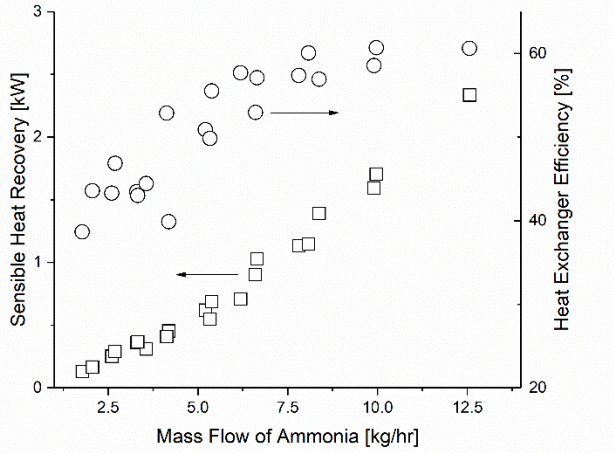

FIGURE 7: HEAT RECOVERY RATE AND HEAT EXCHANGER EFFICIENCY FOR THE TCR REACTOR.

3.2 Thermochemical Recuperation

Figure 8 shows both the exhaust-side reactor inlet temperatures and energy recuperation as a function of mode and FEF. Exhaust inlet temperatures were found to scale with engine load, with similar outlet temperatures for mode pairs 1 and 5, 3 and 6, and 4 and 7. As load increased, combustion became less lean and combustion temperatures increased. Higher combustion temperatures led to the increased exhaust temperatures seen the experimental measurements. Increased fumigation also increased exhaust temperature across every mode due to the reclaimed sensible energy from the fumigant. Fumigation resulting in lowered air-fuel ratio (AFR) or decreased thermal efficiency of the combustion cycle would also result in higher exhaust temperatures. Higher initial intake charge temperatures produced higher peak in-cylinder temperatures which increased the exhaust temperature.

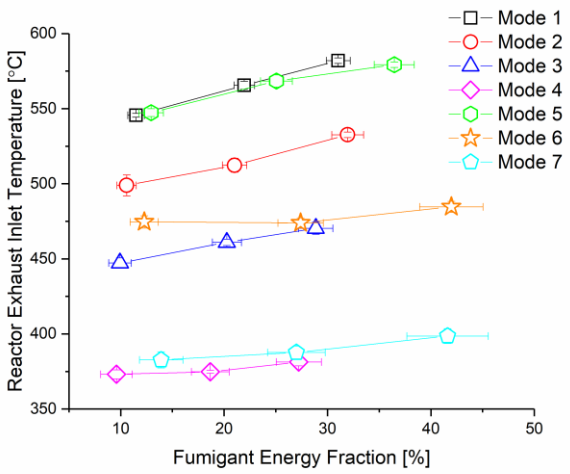

FIGURE 8: EXHAUST TEMPERATURES MEASURED AT THE INLET TO THE TCR REACTOR AS A FUNCTION OF FEF FOR ALL MODES.

Thermochemical heat recovery rate was calculated as the net increase in lower heating value of the fumigant fuel as it passed through the reactor. Figure 9 shows the chemical heat recovery rate by the TCR reactor as a function of mode and FEF. With the exception of mode 1, trends show linear behavior with increasing FEF. Flat or decreasing recovery with increasing FEF is seen in modes 2-4, 6, and 7. This indicates thermally limited kinetics for which additional fumigation does not yield additional hydrogen production. Higher ammonia flow rates increase heat exchange coefficients within the reactor, but also decrease residence times and increase the rate at which sensible energy is removed from the reactor. Depending on the inlet ammonia temperature, the decomposition catalyst may decrease in temperature. This decreases catalyst activity and hydrogen yield. For mode 5, high exhaust temperatures and lower ammonia flows allowed for increasing recovery as fumigation increased. Conversion efficiency was high at low FEF and high temperature. The reaction caused a rapid decrease in ammonia mole fraction, causing conversion rates to decrease by the catalyst exit. Increased fumigation decreased conversion efficiency but produced more hydrogen by mass from the fumigant stream.

Total recovered energy scaled with the rate of production of hydrogen, and thus higher flows increased recovered energy. Low recovery was calculated for modes 4 and 7, which also showed the lowest measured exhaust temperatures. These temperatures are near the minimum required for catalytic ammonia decomposition activity, suggesting that any further decrease would cause the reaction to cease. The catalyst temperature was also dependent on the monolith geometry and heat transfer effects. While this TCR reactor is limited at temperatures below 350 °C, activity at lower temperatures is possible with improvements to the reactor's thermal design.

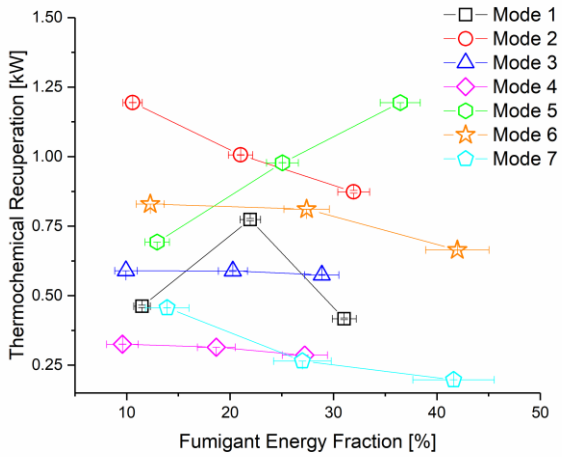

FIGURE 9: THERMOCHEMICAL RECUPERATION RATE AS A FUNCTION OF FEF FOR ALL MODES.

The chemical energy recovered by the TCR reactor decreased the total heating value input needed to produce a given engine power output. This corresponded to an increase in engine brake thermal efficiency, which is plotted as a function of mode and FEF in figure 10. Modes 1, 2, 5-7 showed increased BTE with increased ammonia fumigation indicating net thermochemical recuperation was achieved. Decreases in brake thermal efficiency noted in modes 3 and 4 were caused by poor conversion efficiency through the decomposition catalyst accompanied by decreased combustion efficiency. Unburned ammonia emissions represent lost heating value which exceeds the additional energy provided by TCR. Mode 1 and 5 show a maximum benefit to BTE at 10% replacement. This was due to low flow causing high conversion efficiency in the reactor and leading to high chemical energy recovery with lower flow rates of ammonia. Unburned ammonia emissions also decreased with high conversion as some ammonia was converted to hydrogen before the combustion event. Intake hydrogen molar concentration was calculated based on the conversion efficiency and reformate mass flow rate. The hydrogen concentrations are

reported in figure 11 and showed the same trends as the thermochemical recuperation rate.

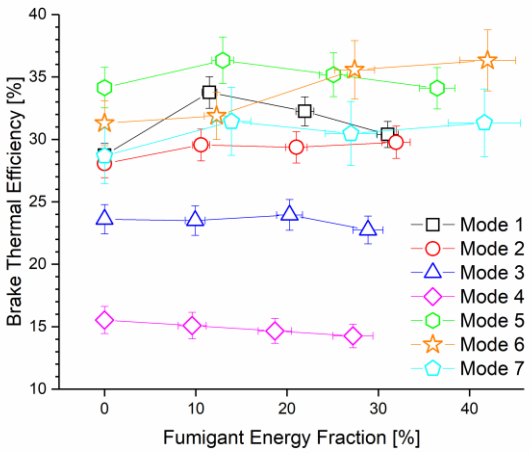

FIGURE 10: BRAKE THERMAL EFFICIENCY VS. FEF FOR ALL MODES.

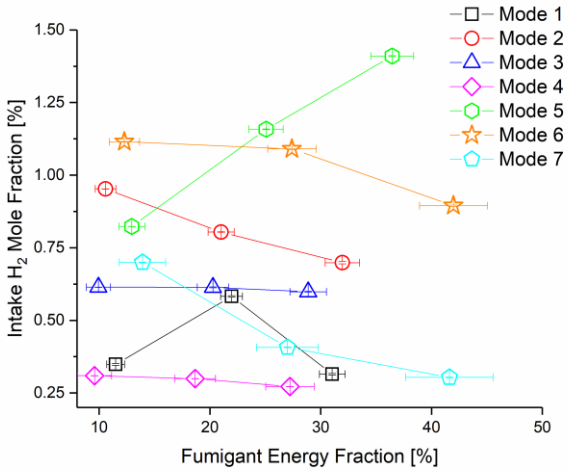

FIGURE 11: INTAKE CHARGE H_2 MOLAR CONCENTRATION AS A FUNCTION OF FEF FOR ALL MODES.

A first law analysis was performed for the TCR system. The results are depicted in the two Sankey diagrams shown in figures 12 and 13. The figures show the 0% and 30% FEF cases, respectively for mode 5. Using the ammonia TCR system, 30% FEF resulted in a net measured BTE increase from 33.4% to 34.1%. Total recovered energy rate was calculated to be 7.8 kW which resulted in a fuel energy decrease of 3.1 kW. Thermal energy recovered by the TCR system was recycled into the engine thermodynamic cycle but did not reduce fuel energy input as chemically recovered energy did. However, the increased thermal energy served to increase in-cylinder combustion temperatures by heating the intake charge. This resulted in faster combustion kinetics for diesel and ammonia and increased combustion efficiency. Higher combustion temperatures also produced higher NO_x levels through the thermal mechanism. While thermal and combustion efficiencies both showed a measured increase, they were only realized with a marked increase in harmful emissions. In modern engines, the energy expended on aftertreatment for this additional NO_x may negate the benefit of the efficiency gains.

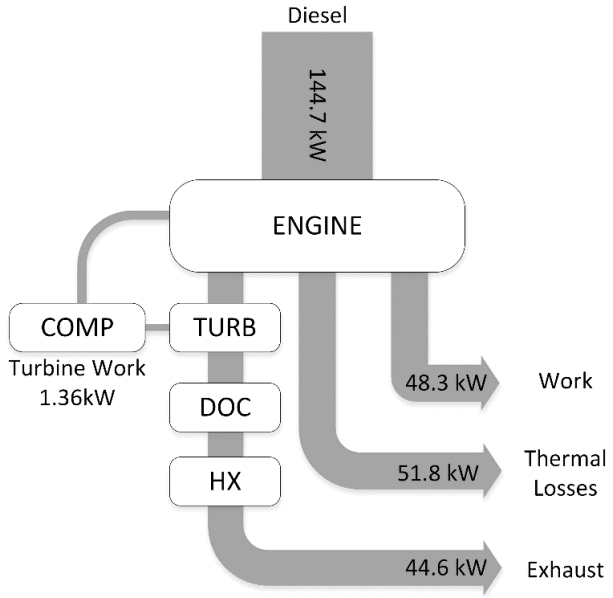

FIGURE 12: SANKEY DIAGRAM FOR MODE 5 CDC.

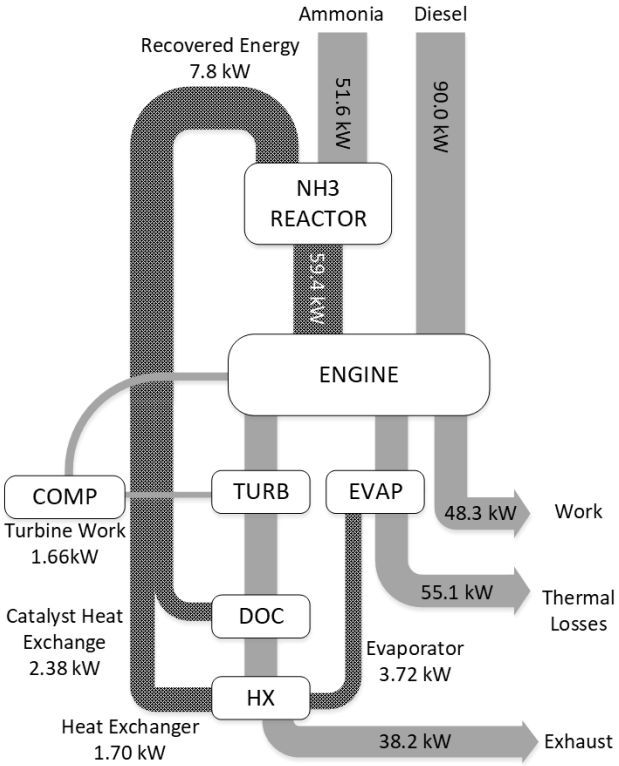

FIGURE 13: SANKEY DIAGRAM FOR MODE 5 WITH 30% AMMONIA REPLACEMENT.

3.3 Emissions Analysis

Ammonia contains no carbon; therefore, engine CO_2 emissions decreased linearly with increasing FEF as depicted in figure 14. CO_2 emissions also decreased on a brake-specific basis due to increasing engine efficiency for modes 1, 2, 6, and 7. Despite this, modes where efficiency decreased due to fumigation still show CO_2 emissions benefit when ammonia replaces diesel fuel.

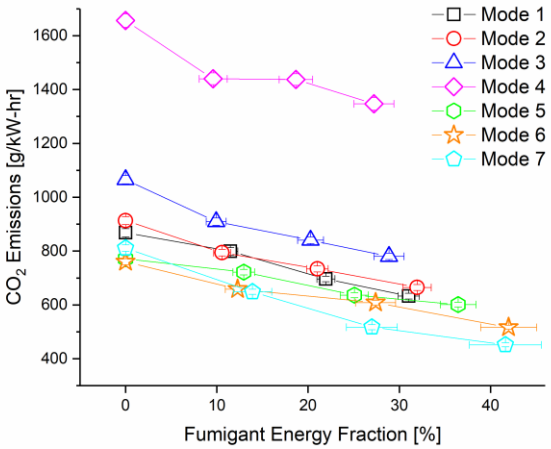

FIGURE 14: BRAKE SPECIFIC CO_2 EMISSIONS VS. FEF FOR ALL MODES.

Figure 15 shows the trends for brake specific soot emissions as a function of mode and FEF. The EPA Tier-4 final limit is shown as a horizontal black bar and is adjusted by a factor of 0.5 to account for the soluble organic fraction of particulate matter [30,31]. Soot emissions increased strongly ammonia fumigation for some modes, with only mode 6 and 7 showing a decrease by 30% FEF. Mode 1, 2, and 5 show decreases from baseline before increasing by 30% FEF. Increasing soot trends can be explained by the ammonia's effect on the intake charge.

When ammonia was fumigated into the intake stream, the intake manifold pressure increased slightly. The increased pressure upstream of the compressor would cause decreased air mass flow rate. This, in turn, decreased the mole fraction of oxygen in the charge and also decreased the AFR slightly. When diesel was injected into the intake charge near top dead center, the fuel burned diffusively. The local equivalence ratio of the diffusion flame was increased with increased ammonia fuel present in the intake charge. However, since ammonia combustion cannot directly produce soot, emissions were reduced with increasing FEF due to the displacement of diesel fuel with ammonia.

Decreasing soot emissions at intermediate FEF levels were caused by displacement of carbon in the diesel fuel, but also the increase in BTE with these levels of fumigation. The hydrogen fraction of the fumigant fuel would enhance flame propagation in the case of intermediate FEF levels and could serve to promote both turbulent mixing increase diesel combustion kinetics. The former of which would lower local equivalence ratio in the diesel flame, whereas the latter could serve to either promote or retard soot production depending on the timing of the hydrogen-ammonia combustion relative to the diesel combustion.

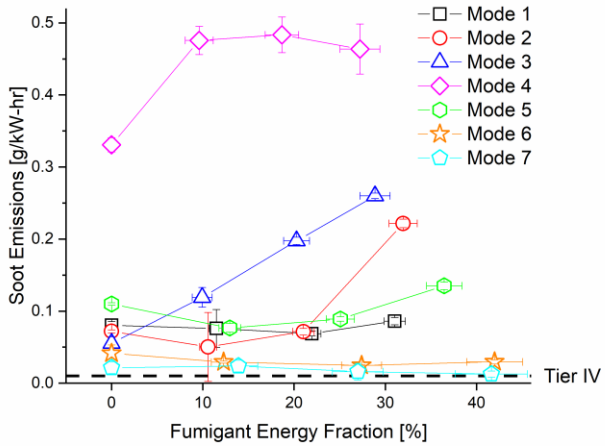

FIGURE 15: BRAKE SPECIFIC SOOT EMISSIONS AS A FUNCTION OF FEF FOR ALL MODES. TIER FOUR LIMIT SHOWN AS DASHED LINE

Ammonia combustion is known to increase engine NO_x emissions due to fuel-bound nitrogen atoms. This production phenomenon is called fuel-NO_x and was shown to occur in all measurements in this study. Shown in figure 16, all seven modes show increasing NO_x emissions with FEF and all tested points exceed the even the initial EPA tier-1 emissions standards. This was expected as the experimental engine predates the tier-1 standard. However, excluding modes 3 and 4, most modes remained near their diesel-only baseline values. This is due to the high ammonia dissociation through the reformer at high engine load that reduced the concentration of ammonia in the intake charge. NO_x emissions increased with fumigation for modes 3 and 4 due to the poor conversion of ammonia within the TCR reactor. Fumigated fuel consisted of unconverted ammonia, which burns inefficiently without hydrogen to promote flame propagation. Lean conditions prevented fuel-NO_x from oxidizing other fuel, and it is exhausted from the cylinder unreduced. Rhodium-based catalysts have been long-known to selectively oxidize ammonia to NO_x under lean conditions such as diesel exhaust. [32] Due to similar catalyst formulation, the diesel oxidation catalyst within the TCR reactor was also expected to convert some unburned ammonia to additional NO_x. This conversion further increased the measured emissions.

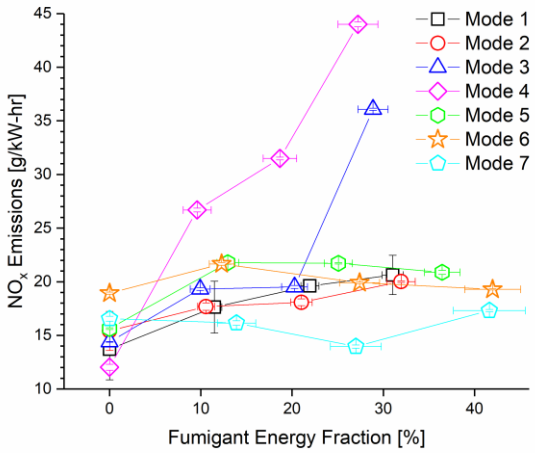

FIGURE 16: BRAKE SPECIFIC NO_X EMISSIONS FEF FOR ALL MODES.

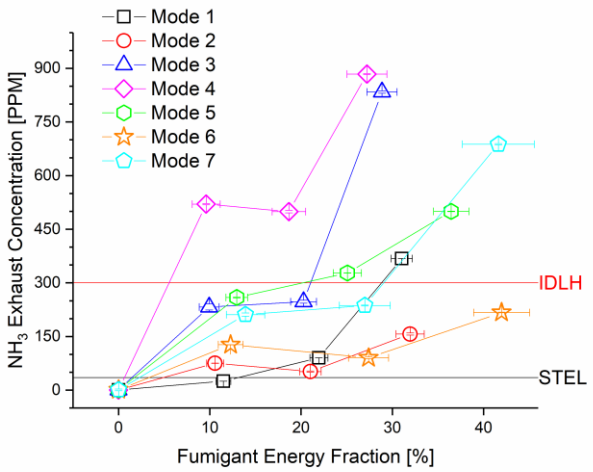

FIGURE 17: PPM NH_3 EMISSIONS FEF FOR ALL MODES. NIOSH IMMEDIATE DANGER TO LIFE AND HEALTH LEVEL AND SHORT TERM (15 MINUTE) EXPOSURE LEVELS ARE SHOWN AS HORIZONTAL BARS. [33]

Ammonia slip through the system was measured and is reported in figure 17. Increased fumigation resulted in increased levels of ammonia exhaust emissions, with the lowest brake specific emissions resulting from the modes with highest TCR activity. Ammonia's poor flame propagation was enhanced by the presence of hydrogen, higher temperatures, and richer combustion. It serves to reason in this case that higher ammonia emissions were likely a stronger function of lower hydrogen concentration in the intake manifold, as increasing fumigation would increase intake charge temperature and increase premixed charge equivalence ratio. The TCR reactor used a diesel oxidation catalyst which oxidized unburned ammonia. Higher temperatures enhanced the rate of ammonia oxidation. Exhaust temperatures were shown to increase with engine load, as was engine brake thermal efficiency. For this reason, brake specific ammonia emissions are highest for modes with low efficiency and low exhaust temperature. Modes 3 and 4 are high speed and low load conditions which are unlikely long-term operating points for an agricultural tractor. For a dynamic fueling system installed on such a vehicle, high specific ammonia emissions could be eliminated by fueling these modes with diesel only.

4. CONCLUSION

In this work, an ammonia-diesel dual fuel TCR reactor system was demonstrated on a tractor. The tractor was operated over a standard 8-mode test and fueled with ammonia at FEF of 10-30%. The system demonstrated both thermal and chemical recuperation using an ammonia decomposition reactor and produced hydrogen fuel from the ammonia. Brake thermal efficiency was improved for most modes due to reclaimed energy in hydrogen production and more efficient ammonia combustion due to the effect of hydrogen flame-speed enhancement.

First-law analysis showed that both chemical and thermal energy was reclaimed effectively by the TCR system. Benefits to engine efficiency were realized though recovery of waste thermal and chemical energy. Thermal energy was shown to be recycled into the engine intake charge through fumigant, though the direct effect on combustion remains unclear. Conversion efficiency of the ammonia TCR reactor was below 50% for all 30% FEF cases, indicating the need for more efficient heat transfer or larger reactor volume to accommodate further recuperation.

Emissions from the engine under CDC and ammonia fumigation were measured. CO_2 emissions were shown to decrease due to the replacement of hydrocarbon fuel with carbon-free ammonia. Soot emissions showed an increasing trend with fumigation, as did both NO_x and ammonia emissions. Low temperature exhaust at low-load conditions decreased the conversion efficiency of ammonia and increased the brake specific emissions of ammonia and NO_x. High brake-specific ammonia and NO_x emissions at these conditions can be eliminated if fumigation is used selectively. Fumigating only at medium and high loads would both increase TCR rates per unit ammonia consumed, and lower average emissions by avoiding

high-emission conditions entirely. In the case that NO_x formation and ammonia slip were still excessive, use of selective catalytic reduction either within the TCR reactor or downstream on the exhaust side would eliminate both the ammonia and NO_x simultaneously. By using only unburned ammonia in the exhaust stream, this passive process would decrease both emissions without increasing ammonia consumption.

These findings indicated feasibility for both ammonia-diesel dual-fuel engines and TCR systems for commercial vehicles. Energy recuperation increased brake thermal efficiency for most modes, but low total ammonia conversion suggests much greater capacity for recuperation. Increased recuperation would be realized by more efficient heat exchange, which allows the TCR reaction to proceed at higher temperatures and faster rates. Higher catalyst loading or more active catalyst formulations would also produce greater conversion rates. Future work will explore these designs to improve both efficiency and emissions of ammonia TCR systems.

ACKNOWLEDGEMENTS

This project was sponsored by the Legislative Citizen Commission on Minnesota Resources under M.L. 2016, Chp. 186, Sec. 2, Subd. 07c. We would like to thank our colleagues at the University of Minnesota West Central Research and Outreach Center for providing the tractor used in this work. We would also like to thank our colleagues at the University of Wisconsin River Falls Agricultural Engineering program for providing the PTO dynamometer used in this work. Finally, we would like to acknowledge Andrew York and David Wails of Johnson Matthey, Plc for coating the catalyst assembly used in this work.

REFERENCES

[1] Reese, M., Marquart, C., Malmali, M., Wagner, K., Buchanan, E., McCormick, A., and Cussler, E. L., 2016, "Performance of a Small-Scale Haber Process," Ind. Eng. Chem. Res., **55**(13), pp. 3742–3750.

[2] Kobayashi, H., Hayakawa, A., Somarathne, K. D. K. A., and Okafor, E. C., 2019, "Science and Technology of Ammonia Combustion," Proc. Combust. Inst., **37**(1), pp. 109–133.

[3] Frigo, S., Gentili, R., and De Angelis, F., 2014, "Further Insight into the Possibility to Fuel a SI Engine with Ammonia plus Hydrogen," SAE Tech. Pap., **1**(2014-32–0082).

[4] Frigo, S., and Gentili, R., 2013, "Analysis of the Behaviour of a 4-Stroke Si Engine Fuelled with Ammonia and Hydrogen," Int. J. Hydrogen Energy, **38**(3), pp. 1607–1615.

[5] Pozzana, G., Bonfanti, N., Frigo, S., Doveri, N., Dario, P., Mattoli, V., and Ragnoli, M., 2012, "A Hybrid Vehicle Powered by Hydrogen and Ammonia."

[6] Comotti, M., and Frigo, S., 2015, "Hydrogen Generation System for Ammonia-Hydrogen Fuelled Internal Combustion Engines," Int. J. Hydrogen Energy, **40**(33), pp. 10673–10686.

[7] Grannell, S. M., Assanis, D. N., Bohac, S. V., and Gillespie, D. E., 2008, "The Fuel Mix Limits and Efficiency of a Stoichiometric, Ammonia, and Gasoline Dual Fueled Spark Ignition Engine," J. Eng. Gas Turbines Power, **130**(4), p. 042802.

[8] Haputhanthri, S. O., 2014, "Ammonia Gasoline Fuel Blends: Feasibility Study of Commercially Available Emulsifiers and Effects on Stability and Engine Performance," SAE Tech. Pap. Ser., **1**, pp. 0–5.

[9] Reiter, A. J., and Kong, S. C., 2008, "Demonstration of Compression-Ignition Engine Combustion Using Ammonia in Reducing Greenhouse Gas Emissions," Energy & Fuels, **22**(5), pp. 2963–2971.

[10] Reiter, A. J., and Kong, S. C., 2011, "Combustion and Emissions Characteristics of Compression-Ignition Engine Using Dual Ammonia-Diesel Fuel," Fuel, **90**(1), pp. 87–97.

[11] Otomo, J., Koshi, M., Mitsumori, T., Iwasaki, H., and Yamada, K., 2018, "Chemical Kinetic Modeling of Ammonia Oxidation with Improved Reaction Mechanism for Ammonia/Air and Ammonia/Hydrogen/Air Combustion," Int. J. Hydrogen Energy, **43**(5), pp. 3004–3014.

[12] Kobayashi, H., Hayakawa, A., Somarathne, K. D. K. A., and Okafor, E. C., 2019, "Science and Technology of Ammonia Combustion," Proc. Combust. Inst., **37**(1), pp. 109–133.

[13] Hill, A. K., and Torrente-Murciano, L., 2014, "In-Situ H2 Production via Low Temperature Decomposition of Ammonia: Insights into the Role of Cesium as a Promoter," Int. J. Hydrogen Energy, **39**(15), pp. 7646–7654.

[14] Hill, A. K., and Torrente-Murciano, L., 2015, "Low Temperature H2 Production from Ammonia Using Ruthenium-Based Catalysts: Synergetic Effect of Promoter and Support," Appl. Catal. B Environ., **172**–**173**, pp. 129–135.

[15] Huang, D. C., Jiang, C. H., Liu, F. J., Cheng, Y. C., Chen, Y. C., and Hsueh, K. L., 2013, "Preparation of Ru-Cs Catalyst and Its Application on Hydrogen Production by Ammonia Decomposition," Int. J. Hydrogen Energy, **38**(8), pp. 3233–3240.

[16] Plana, C., Armenise, S., Monzón, A., and García-Bordejé, E., 2010, "Ni on Alumina-Coated Cordierite Monoliths for in Situ Generation of CO-Free H2 from Ammonia," J. Catal., **275**(2), pp. 228–235.

[17] Aika, K. ichi, 2017, "Role of Alkali Promoter in Ammonia Synthesis over Ruthenium Catalysts—Effect on Reaction Mechanism," Catal. Today, **286**, pp. 14–20.

[18] Bajus, S., Agel, F., Kusche, M., Ní Bhriain, N., and Wasserscheid, P., 2016, "Alkali Hydroxide-Modified Ru/γ-Al2O3 Catalysts for Ammonia Decomposition," Appl. Catal. A Gen., **510**, pp. 189–195.

[19] Yin, S. F., Xu, B. Q., Wang, S. J., and Au, C. T., 2006, "Nanosized Ru on High-Surface-Area Superbasic ZrO2-KOH for Efficient Generation of Hydrogen via

Ammonia Decomposition," Appl. Catal. A Gen., **301**(2), pp. 202–210.
[20] Hwang, J., Li, X., and Northrop, W., 2017, "Exploration of Dual Fuel Diesel Engine Operation with On- Board Fuel Reforming."
[21] Tsolakis, A., and Megaritis, A., 2004, "Catalytic Exhaust Gas Fuel Reforming for Diesel Engines - Effects of Water Addition on Hydrogen Production and Fuel Conversion Efficiency," Int. J. Hydrogen Energy, **29**(13), pp. 1409–1419.
[22] Tsolakis, A., Megaritis, A., and Yap, D., 2008, "Application of Exhaust Gas Fuel Reforming in Diesel and Homogeneous Charge Compression Ignition (HCCI) Engines Fuelled with Biofuels," Energy, **33**(3), pp. 462–470.
[23] Fennell, D., Herreros, J. M., Tsolakis, A., Xu, H., Cockle, K., and Millington, P., 2013, "GDI Engine Performance and Emissions with Reformed Exhaust Gas Recirculation (REGR)," (Equation 3).
[24] Engelhardt, P., Maximini, M., Beckmann, F., Brenner, M., and Moritz, O., 2014, "Coupled Operation of a Diesel Steam Reformer and an LT- and HT-PEFC," Int. J. Hydrogen Energy, **39**(31), pp. 18146–18153.
[25] Kopasz, J. P., Miller, L. E., and Ahmed, S., 2016, "Reforming Petroleum-Based Fuels for Fuel Cell Vehicles : Composition-Performance Relationships," (724).
[26] Chen, J., Yan, L., Song, W., and Xu, D., 2016, "Operating Strategies for Thermally Coupled Combustion-Decomposition Catalytic Microreactors for Hydrogen Production," Int. J. Hydrogen Energy, **41**(46), pp. 21532–21547.
[27] Heywood, J. B., 1988, *Internal Combustion Engine Fundamentals*, McGraw-Hill, New York.
[28] Rathore, S. S., Singh, A., Kumar, P., Alam, N., Sahu, M. K., and R, S., 2018, "Review of Exhaust Gas Heat Recovery Mechanism for Internal Combustion Engine Using Thermoelectric Principle," SAE Tech. Pap. Ser., **1**(2011), pp. 1–10.
[29] Bell, I. H., Wronski, J., Quoilin, S., and Lemort, V., 2014, "Pure and Pseudo-Pure Fluid Thermophysical Property Evaluation and the Open-Source Thermophysical Property Library Coolprop," Ind. Eng. Chem. Res., **53**(6), pp. 2498–2508.
[30] Vitaly Y. Prikhodko, Scott J. Curran, Teresa L. Barone, Samuel A. Lewis, John M. Storey, Kukwon Cho, Robert M. Wagner and James E. Parks, I., 2011, "Diesel Oxidation Catalyst Control of Hydrocarbon Aerosols From Reactivity Controlled Compression Ignition Combustion," ASME Int. Mech. Eng. Congr. Expo., **9**, pp. 273–278.
[31] 2019, "Nonroad Diesel Engine EPA Emissions Standards," DieselNet [Online]. Available: https://www.dieselnet.com/standards/us/nonroad.php.
[32] Handforth, S. L., and Tilley, J. N., 1934, "Catalysts for Oxidation of Ammonia to Oxides of Nitrogen," Ind. Eng. Chem., **26**(12), pp. 1287–1292.
[33] 2019, "NIOSH Pocket Guide to Chemical Hazards" [Online]. Available: https://www.cdc.gov/niosh/npg/.